A NON-PARAMETRIC CHANGE DETECTION METHOD FOR ROCKFALL MONITORING

IOANNIS FARMAKIS [1], DAVIDE ETTORE GUCCIONE [1], KLAUS THOENI [1], ANNA GIACOMINI [1]

[1] *Centre for Geotechnical Science and Engineering, The University of Newcastle, Australia,* i.farmakis@icloud.com

Introduction

Rockfall monitoring defines the process of recording rockfall activity patterns along a given rock slope. With 3D data capturing techniques, a typical digital change detection methodology for rockfalls includes three steps – distance computation, spatial clustering, and shape reconstruction (Abellan et al. 2009). Distance computation refers to the computation of distances between two point clouds. A statistical limit of detection at 95% confidence (LoD_{95}) applies to extract significant changes (DiFrancesco et al. 2020). In the second step, the significant distances point cloud should be clustered in space to form individual rockfall point clouds. The third step of the 3D rockfall state-of-the-art methodology includes the computation of the loss volume represented by each individual rockfall point cloud as extracted by spatial clustering (DiFrancesco et al. 2021). This state-of-the-art methodology includes some user-defined input parameters at each step that can significantly influence the result. The selection of appropriate input parameter values within the individual steps of the process poses specific challenges associated with the nature of the problem and the data type. This is mainly because rockfalls as phenomena can occur in any size and arrangement and thus configurations made for specific block sizes and patterns may not always apply to the entire extent of the monitored rock slope. Considering the several challenges associated with user-defined parameter selection within the distance-based state-of-the-art 3D rockfall detection methodology, this paper presents a non-parametric method specifically designed for 3D rockfall monitoring.

Methods

The new method, VoxFall (voxelized rockfall), does not rely on any distance computation and its objective is to eliminate user subjectivity and present a new tool for rockfall monitoring that would only be controlled by the quality of the input data. VoxFall's development was based on the following three conceptual principles: a) in rockfall detection the interest is not in the magnitude or the direction of the displacement of each point but in the volume that has been detached (not displaced), b) as in an image, where anything below the resolution is not visible, VoxFall uses a voxel (volumetric pixel) grid – a 3D image of the scene – which's resolution is defined by the quality properties of the input models, and c) often in rockfall cases model coverage is challenged by the survey setting where it is apparent that volume computations require shape reconstruction of the extracted clusters with hole-filling.

The algorithm treats the two input models as a single scene and conforming with the realization that this is an unavoidable operation, 3D mesh models are used as input. After the required pre-processing the two models are merged and the rockfall volumes are enclosed between the "before" and "after" surfaces (Figure 1a, b). However, it is important to make sure that the detected clusters of the empty space satisfy a minimum degree of confidence and do not include the effects of potentially insufficient data quality. To achieve that, we apply a two-step process:

1) **Fitting an occupancy grid:** To extract the empty space from the input scene we use a voxel (volumetric pixel) grid (Figure 1c). VoxFall is a non-parametric method where the resolution of the analysis (voxel size) – which is the only factor that could influence the result – is defined by the quality of the input data, and specifically by the registration error. To extract the empty space between the two models, we need to make sure that there are no empty voxels between stable parts. Therefore, the quality of the input data decides the ability of VoxFall to reliably only "see" the empty space that corresponds to rockfalls and confidently avoid false positives.
2) **Empty space clustering and volume computation:** By using the voxel grid data structure, we cluster the extracted continuous 3D space without relying on any input parameter. Spatial

clustering in VoxFall is simple and neighbor search is facilitated by grid indexing. For each rockfall cluster, the volume is computed as a function of the voxels it includes.

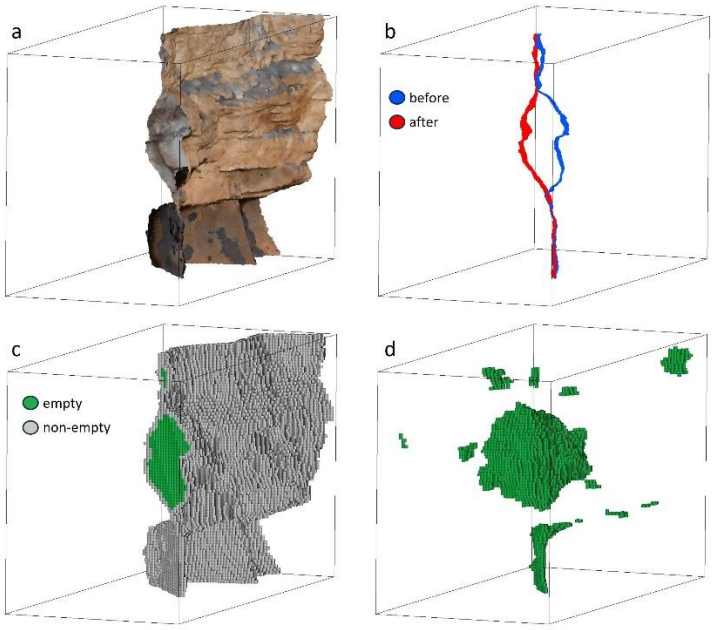

Figure 1. VoxFall detection method.

Results and Conclusions

To validate the reliability of the new algorithm a synthetic seting and real rock slope dataset were used. VoxFall performance was compared to the existing distance-based methodologies. The results across all the experimental settings prove the sensitivity of the distance-based methods and the dependency of the detections on the input parameters compared to VoxFall detections. Specifically, distance-based rockfall detection workflows appear to be highly sensitive to not only the spatial clustering tuning but also their distance computation input parameters. In the original dataset, VoxFall almost perfectly predicts the rockfall volume (0.3% difference) within an arrangement of recorded rockfall events.

The study conludes that distance-based rockfall monitoring as it is used today is highly sensitive to multiple input parameters and requires pre-existing knowledge of rockfall activity to tune them. The new method – VoxFall – provides a unified framework that enables for direct volume detection and clustering amongst them. VoxFall results depend only on the input data quality and no user intervention is required. The study's comprehensive experiments support that VoxFall can provide high quality results in terms of both segmentation/detection and volume estimation introducing the method as an efficient and effective tool for 3D rockfall monitoring.

References

Abellán, A., Jaboyedoff, M., Oppikofer, T., Vilaplana, J.M., 2009. Detection of millimetric deformation using a terrestrial laser scanner: experiment and application to a rockfall event. Nat. Hazards Earth Syst. Sci. 9, 365–372. https://doi.org/10.5194/nhess-9-365-2009

DiFrancesco, P.-M., Bonneau, D., Hutchinson, D.J., 2020. The Implications of M3C2 Projection Diameter on 3D Semi-Automated Rockfall Extraction from Sequential Terrestrial Laser Scanning Point Clouds. Remote Sens. 12, 1885. https://doi.org/10.3390/rs12111885

DiFrancesco, P.-M., Bonneau, D.A., Hutchinson, D.J., 2021. Computational Geometry-Based Surface Reconstruction for Volume Estimation: A Case Study on Magnitude-Frequency Relations for a LiDAR-Derived Rockfall Inventory. ISPRS Int. J. Geo-Information 10, 157. https://doi.org/10.3390/ijgi10030157

FLUID FLOW CAPABILITY OF INCIPIENT FOLIATION, NATURAL FRACTURE ALONG FOLIATION, AND TENSILE FRACTURES OF SLATE

XUAN-XINH NGUYEN [1], CHE-WEI YEH [2] TAN-MINH LE [2], JIA-JYUN DONG [2,3]

[1] *Institute of Rock Structure and Mechanics, the Czech Academy of Sciences, Prague, Czech Republic, nguyen@irsm.cas.cz*

[2] *Graduate Institute of Applied Geology, National Central University, Taoyuan, Taiwan, n111624006@g.ncu.edu.tw*

[2] *Graduate Institute of Applied Geology, National Central University, Taoyuan, Taiwan, minhpro84@gmail.com*

[2] *Graduate Institute of Applied Geology, National Central University, Taoyuan, Taiwan, jjdong@geo.ncu.edu.tw*

[3] *Earthquake-Disaster & Risk Evaluation and Management Center, National Central University, Taoyuan, Taiwan*

Introduction

Slate host rock relying on induced fractures for enhanced fluid flow in a low permeability system are investigated as a potential CO_2 sequestration and geothermal site. The permeability properties of incipient foliations, fractures along foliation are assessed using slate samples from the Hungyeh Formation in Taiwan. Hydraulic and mechanical apertures (e, E) of both natural and artificial tensile fractures along incipient foliations were measured simultaneously using the pulse-decay-balance (PDB) method based on the YOKO2 system (Nguyen et al., 2023). Stress-dependent hydraulic and mechanical apertures are then applied to determine rock mass permeability using Snow's model (Snow, 1965). The results are compared to the stress-dependent permeability of the matrix to understand the influence of fractures along incipient foliations on reservoir fluid flow behavior.

Methods

Intact slate samples oriented perpendicular and parallel to incipient foliations were drilled from rock cores. Samples drilled parallel to incipient foliations were used to determine natural fracture along foliation (NFF), and create artificial tensile fracture (ATF) using the Brazilian tensile test.

The matrix permeability of intact samples was determined using a pulse decay method (Brace et al., 1968), while stress-dependent matrix permeability was assessed using a power law (Dong et al., 2010). Additionally, the e and E of fractures were measured simultaneously by the pulse-decay-balance method (PDB) based on the YOKO2 system (Nguyen et al., 2023). The E was determined from fracture volume measurements, and the e was derived from an analysis of the pressure decay curve. The stress dependence of the apertures was determined using an exponential function (Liu et al., 2004), and the results were used to calculate the equivalent permeability of rock mass using Snow's model. These findings were then compared to the permeability of intact slate (Fig. 1).

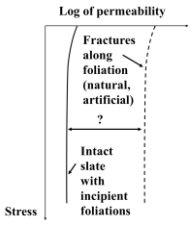

Figure 1. Schematic diagram of stress-dependent permeability of intact slate and fractures along foliation.

Results

Matrix permeability decreases with increasing stress, and anisotropic permeability is observed for incipient foliations. The matrix permeability oriented parallel to incipient foliations (black open circles) is ten times larger than that oriented perpendicular to incipient foliations (gray solid squares) (Fig. 2a).

Permeability of the rock mass increases with decreasing fracture spacing (Snow, 1965). We used an average fracture spacing of 0.1 m, observed from the rock core, to determine the equivalent permeability of rock mass using Snow's model. With smooth joint roughness (joint roughness coefficient, $JRC < 4$) of fractures along foliation, the equivalent permeability of rock mass calculated by the mean stress-dependent e is roughly 0.01–0.1 mD (blue solid curve in Fig. 2d). The contribution of fractures to the permeability is 100 times larger than the matrix permeability. However, the equivalent permeability of rock mass remains within the low permeability range of geothermal reservoirs (light grey region in Fig. 2d). Additionally, assuming the e equals the E for open fractures due to high fluid pressure injection, the equivalent permeability calculated based on the mean stress-dependent E (green solid curve) is approximately 2×10^2–2×10^3 mD (Fig. 2d). The contribution of open fractures to the permeability is 10^4 times greater than that of the matrix permeability (red curve). This significant increase in equivalent permeability places it within the high permeability range (dark gray region in Fig. 2d).

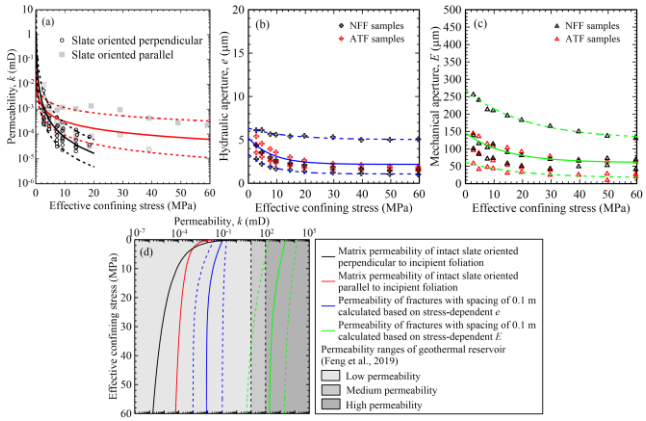

Figure 2. Stress dependency of (a) matrix permeability and (b) $\boldsymbol{e}$ and (c) $\boldsymbol{E}$ of fractures along foliation. (d) The equivalent permeability of rock mass is determined using the Snow's model with spacing of 0.1 m.

Conclusion

Slate host rock with induced fractures for enhanced fluid flow in a low permeability system is a potential site for CO_2 sequestration and geothermal applications. Fluid flow occurs in fractures along incipient foliation under effective stress up to 60 MPa. The equivalent permeability of rock mass with open fractures can increase significantly based on the stress-dependent mechanical aperture.

References

Brace, W. F.; Walsh, J. B.; Frangos, W. T. Permeability of granite under high pressure. *Journal of Geophysical research*. 1968, 73, 2225–2236.

Dong, J. J.; Hsu, J. Y.; Wu, W. J.; Shimamoto, T.; Hung, J. H.; Yeh, E. C.; Wu, Y. H.; Sone, H. Stress-dependence of the permeability and porosity of sandstone and shale from TCDP Hole-A. *International Journal of Rock Mechanics and Mining Sciences*. 2010, 47, 1141–1157.

Feng, J. Y.; Zhang, Y.; He, Z. L.; Sun, Z. M.; Luo, J. Discussion on evaluation methodology of hydrothermal geothermal reservoir. *Journal of Groundwater Science and Engineering*. 2019, 7.

Liu, H. H.; Rutqvist, J.; Zhou, Q.; Bodvarsson, G. S. Upscaling of normal stress-permeability relationships for fracture networks obeying fractional Levy motion. *Elsevier Geo-Engineering Book Series*. 2004, 2, 263–268.

Nguyen, X. X.; Tai, P. L.; Dong, J. J.; Yu, C. W. A novel pulse-decay-balance method for smooth rock joint aperture measurement. *International Journal of Rock Mechanics and Mining Sciences*. 2023, 170, 105504.

Snow, D. T. *A parallel plate model of fractured permeable media*. Ph.D. Thesis, University of California, Berkeley, California, USA, 1965.

CASE STUDY ON USING OPTICAL SENSORS TO INVESTIGATE GROUNDWATER FLOW VELOCITY AND DIRECTION

CHIHPING KUO [1], CHENYU YANG [2]

[1] *National Yunlin University of Science and Technology, Taiwan, Taiwan, cpkuo@yuntech.edu.twl*

[2] *National Yunlin University of Science and Technology, Taiwan, Taiwan, M11216009@yuntech.edu.tw*

Abstract

Detecting groundwater flow velocity and direction is an important work for hydrogeological and geotechnical engineering. Many methods were developed and are used now, such as thermal sensors, electromagnetic sensors, ultrasonic sensors, impeller sensors, and so on. In this study, optical sensors were used to investigate the situation of in-situ groundwater. The methodology of such kinds of sensors is to detect the suspended particles in the fluid and count their velocity and velocity. The results of the sensors compared with the customized environmental conditions in the test site were discussed here. A field test was discussed in this study as well.

Study Area

A construction requires dewatering wells for deep excavation. The location of the site is close to the left shore of Keelung River and showed in Figure 1. The average flow of the river is about 3,690cms and the average velocity for normal days is about 0.53m/s. According to geological investigation data, the upper stratum near surface contains interlayers of sandy soil and clayey soil, called Songshan stratum with an average thickness about 40m around the study area. The low stratum beneath Songshan stratum contains gravels, called Chingmei stratun. Chingmei stratum is a confining aquifer containing saturated groundwater. For the deep excavation, the permeability parameter (K) of the gravel, as showen in Figure 2, in Chingmei stratum is required to acquire by in-situ investigation and laboratorial test.

Methods

The permeability parameter is crucial for the design of the pumping wells. However, the permeability parameters were not easy to evaluated by the sample from drilled boreholes because they were disturbed. The boreholes, named #AH-1 and #AH-2, were performed to observe the soil samples and groundwater. The casing pipes with screen at GL-40m to -43m were installed in the boreholes to be observing wells. The outer gap around the depth of screen was filled with fine sands and other area was sealed with bentonite. The sensor uses optical camera to catch motion of particles was employed to evaluate velocity and direction of groundwater flow. According to Darcy's Law, the permeability parameter can be evaluated by velocity (V) and hydraulic gradient (i).

Results

The evaluated velocities of each location is listed in Table 1. The hydraulic gradient (i) was 0.00035, thus the converted permeability parameter (K) is listed in Table 1. As well. The range of permeability parameter (K) is from 1.311 cm/sec to 4.658 cm/sec, the values from #AH-2 is larger than from #AH-1. The value coordinates to the permeability of GP that defined in USCS, say Poorly graded gravel, sandy gravel, with little or no fines.

The direction of groundwater flow is majorly toward north-east as from observing well#AH-2 to #AH-1. The result of the detection of direction matched the evaluation of velocity.

Conclusion

To use optical sensors to investigate groundwater flow velocity and direction is efficient and useful to evaluated permeability parameter (K).

However, the groundwater body that too turbid or too clear is disincentive to this method.

References

Geotech Environmental Equipment, Inc., Introuduction Website of Geotech Colloidal Borescope , https://www.geotechenv.com/geotech_colloidal_borescope.html

Peter M. Kearl, Observations of Particle Movement in a Monitoring Well Using the Colloidal Borescope. *Joumnal of Hydrology*. 1997, 200:323-344.

Kearl, P. M. and Roemer, K., Evaluation of Groundwater Flow Directions in a Heterogencous Aquifer Using the Colloidal Borescope. *Advances in nvironmental Research*. 1998, 2(1), 12-23.

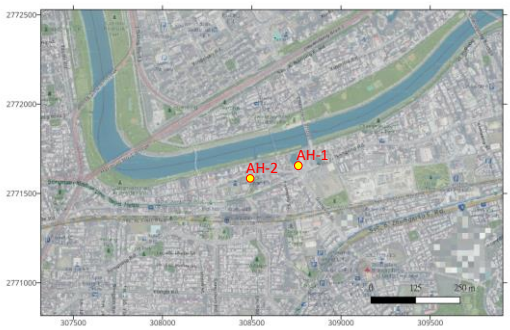

Figure 1. The map of study area and the borehole for observing groundwater

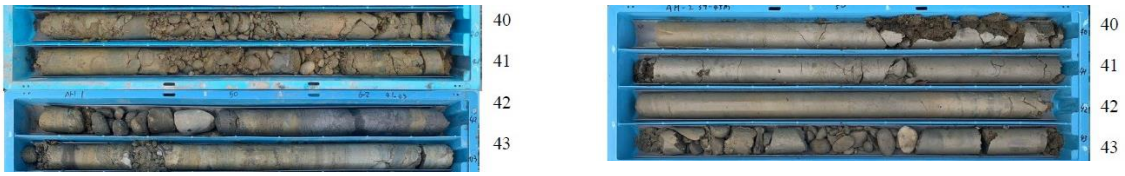

(a) the bored soil and rock samples from BH#AH-1 (b) the bored soil and rock samples from BH#AH-2

Figure 2. The borehole samples of borehole #AH-1 and #AH-2 in Figure 1

(a) the probe of optical camera and lights (b) the performance of the test

Figure 3. The equipment used in this study

Table 1. Measured results of velocity of groundwater and evaluated permeability of the stratum

AH-1			AH-2		
GL-[m]	V(um/sec)	K(cm/sec)	GL-[m]	V(um/sec)	K(cm/sec)
40	466.94	1.311	40	1345.32	3.776
41	648.11	1.819	41	1659.73	4.658
42	635.96	1.785	42	920.73	2.584
43	515.73	1.447	43	1650.35	4.632

GEOHYDROLOGICAL MONITORING OF SLOPE USING ADVANCED DISTRIBUTED FIBRE-OPTIC SENSING: FROM LABORATORY STUDY TO FIELD APPLICATIONS

ASHIS ACHARYA[1,*], DAIKI TANIMURA[2], CHAO ZHANG[3], FUMIHIKO ITO[3], TOSHIHIRO SAKAKI[4], MITSURU KOMATSU[5], ISSEI DOI[6], AND TETSUYA KOGURE[7,8,9]

[1]*Major in Science of Environmental Systems, Graduate School of Natural Science and Technology, Shimane University, 1060 Nishikawatsu-cho, Matsue, Shimane 690-8504, Japan*
[2]*Major in Science and Engineering, Graduate School of Natural Science and Technology, Shimane University, 1060 Nishikawatsu-cho, Matsue, Shimane 690-8504, Japan*
[3]*Interdisciplinary Faculty of Science and Engineering, Shimane University, 1060 Nishikawatsu-cho, Matsue, Shimane 690-8504, Japan*
[4]*ESE Consulting, LLC, 6-10-101 Midorigaokacho, Ashiya, Hyogo 659-0014, Japan*
[5]*Graduate School of Environmental and Life Science, Okayama University, 3-1-1 Tsushimanaka, Kita-ku, Okayama 700-8530, Japan*
[6]*Disaster Prevention Research Institute, Kyoto University, Gokasho, Uji, Kyoto 611-0011, Japan*
[7]*Institute of Environmental Systems Science, Shimane University, 1060 Nishikawatsu-cho, Matsue, Shimane 690-8504, Japan*
[8]*Centre for Natural Disaster Reduction Research and Education, Shimane University, 1060 Nishikawatsu-cho, Matsue, Shimane 690-8504, Japan*
[9]*Disaster Prevention Research Institute, Geodisaster Research Division, Kyoto University, Gokasho, Uji, Kyoto 611-0011, Japan*

Introduction

The development of novel distributed fibre-optic sensing (DFOS) techniques has made significant technological advancements, from traditional slope monitoring tools to real-time measurements of multiple parameters such as strain or temperature (Shi et al. 2021). These sensing methods fulfil the demands of extensive and distributed monitoring of geological structures across vast distances, offering measurements with excellent resolution (Acharya and Kogure 2023). DFOS-based fibre-optic sensors, when embedded into sliding masses, function akin to the nerves in the human body, adeptly capturing extensive information to assess the health condition of the landslide (Acharya and Kogure 2024).

This study evaluated the effectiveness of the Rayleigh-based phase-noise compensated optical frequency-domain reflectometry (PNC-OFDR) method in offering valuable insights into thermal mapping, groundwater flow monitoring, and strain monitoring. A series of experiments were designed and executed to create temperature maps along the length of a test specimen using the PNC-OFDR method, which boasts a fine spatial resolution and rapid measurement times. As a field application, this study attempts to monitor the strain (to examine the deformation characteristics of basement rocks) and temperature changes (to locate the seepage phenomenon) within a deep slope.

Methods

This study demonstrates the feasibility of the PNC-OFDR sensing method to monitor the distributed temperature field with an ultra-short data acquisition period of 2 ms, a spatial resolution of 2 cm, and a temperature resolution of 0.1 °C. Two FR PVC cables were used in the laboratory experiments. One was for heating (heating cable; H-cable), and the other for temperature sensing (temperature measurement cable; T-cable). Two cables were embedded within a cylindrical concrete mortar specimen and subjected to various heating powers. Two water-holding boxes were installed along the specimen at two positions to retain water. If the anomaly of temperature fields is identified with the fibre-optic sensing system by measuring the local spectral shift, the water-supplied position can be located and monitored.

Field deployment involved installing monitoring systems within a 50-meter-deep borehole, where optical cables for heating, temperature sensing, and strain sensing were embedded (Fig.1). The hardened anchorage formed by cement slurry backfill facilitates both seepage detection through actively heated DFOS (AH-DFOS) method and rock deformation monitoring via strain sensing. We have conducted the heating tests of boreholes at different electrical powers to locate the groundwater and other seepage phenomena. We continuously record strain and temperature within the borehole and delve into the relationship between bedrock deformation, seasonal variations, and groundwater flow levels.

Figure. 1 Methods of optical cables installation inside a borehole.

Results

The temporal evolution of temperature along the specimen during a heating period of 3 hrs at four different electrical powers was investigated. The study's results indicated that the PNC-OFDR technique demonstrated a high sensitivity to even small temperature changes, accurately pinpointing water locations at two distinct points. The research determined the minimal heating power required to successfully locate the water positions. The magnitude of the heating power exerted a significant impact on the temperature change. Three distinct phases of temperature increment were observed for a given heating period: rapid, fast, and gentle increase.

DFOS-based cables installed in a deep borehole enabled us to acquire spatially continuous temperature profiles. We measured groundwater dynamics and thermal parameters around a borehole, performing a heating test by heating the armour of a single fibre-optic cable and interpreting the resulting heating curves. We also demonstrated the seasonal effect of the AH-DFOS method on groundwater changes in the context of highly fractured rock.

Conclusion

The experimental study successfully demonstrated the precision of the PNC-OFDR sensing method in monitoring and identifying water position within a two-metre-long cement mortar specimen. Heating the copper wires caused a continuous temperature increase along the specimen, revealing a significant temperature difference between water-supplied and dry sections. Using the AH-DFOS method, we examined groundwater dynamics and the impact of seasonal variations on groundwater levels. Future work will involve continuous strain and temperature monitoring within the borehole, further exploring the relationship between bedrock deformation, seasonal changes, and groundwater flow. The insights and data gathered will benefit engineering geologists and geotechnical engineers in fibre-optic sensing applications for geotechnical monitoring.

References

Acharya, A., Kogure, T. Application of novel distributed fibre-optic sensing for slope deformation monitoring: A comprehensive review. *International Journal of Environmental Science and Technology*. 2023, 8217–8240. https://doi.org/10.1007/s13762-022-04697-5

Acharya, A., Kogure, T. Advances in fibre-optic-based slope reinforcement monitoring: A review, *Journal of Rock Mechanics and Geotechnical Engineering*. 2024 (Accepted on 17 March 2024 for publication)

Shi, B., Zhang, D., Zhu, H., Zhang, C., Gu, K., Sang, H., Han, H., Sun, M., Liu, J. DFOS Applications to geo-engineering monitoring. *Photonic Sensors*. 2021, 11(2):158–186. https://doi.org/10.1007/s13320-021-0620-y

ADVANCEMENTS IN LANDSLIDE VOLUME ESTIMATION: INSIGHTS FROM THE 2016 MW7.8 KAIKOURA EARTHQUAKE

EFSTRATIOS KARANTANELLIS [1], MARIN K. CLARK [1], DIMITRIOS ZEKKOS [2], MIKE J. WILLIS [3]

[1] *Department of Earth and Environmental Sciences, University of Michigan, USA*

[2] *Department of Civil and Environmental Engineering, University of California, USA*

[3] *Department of Geoscience, Virginia Tech, USA*

Introduction

Landslides are complex geological phenomena characterized by the downward movement of mass along a slope. Over the past decades, the frequency and intensity of landslides have been on the rise, primarily due to rapid urbanization, increased occurrence of extreme events, and poor land management practices (Corominas & Moya, 2008). Landslide susceptibility is influenced by factors such as topographical features and engineering geological properties of the rock masses involved (Petley, 2012). Climate change impacts, including changing rainfall patterns and increased weather extremes, have also introduced a new urgency for improving hazard assessment. A common approach involves mapping landslides in 2D using satellite or aerial imagery and estimating the volume by applying a volume-area (V/A) relationship (Larsen et al., 2010). However, the increasing deployment of satellites and the growing accessibility of high-resolution satellite imagery have ignited a new era for landslide volume assessment because of repeat measurements of topography. This study explores the application of satellite photogrammetric technology for landslide volume estimation using 3D change detection procedures. We present a case study of the 2016 Mw7.8 Kaikoura earthquake in New Zealand, which triggered extensive landslides. We utilized high-resolution Digital Surface Models (DSMs) derived from Worldview-3 satellite imagery acquired before and after the earthquake using the SETSM (Surface Extraction with TIN-based Search-space Minimization) algorithm. 3D change detection is employed to estimate landslide volumes across a selected area of interest in Hapuku area, NZ.

The 2016 Mw7.8 Kaikoura Earthquake

The 2016 Mw7.8 Kaikoura earthquake occurred on November 14, 2016, near the town of Kaikoura in the northeastern South Island of New Zealand. The complex earthquake ruptured more than 21 individual fault structures, leading to extensive landsliding (Hamling et al., 2017). The seismic shaking, combined with steep topography and friable geological formations, mobilized large volumes of rock, soil, and debris (Massey et al., 2018, 2020). The 29,557 landslides triggered by the Kaikoura earthquake ranged from shallow soil slips to deep-seated rock failures, causing widespread disruption to transportation networks and infrastructure.

Methods and Results

The SETSM algorithm is an automated object-space digital surface creation algorithm for rational function model imagery, optimized for high-resolution satellite imagery (Noh & Howat, 2015). It generates high-resolution DSMs from stereoscopic satellite imagery by detecting and matching corresponding image features in stereo image pairs to calculate parallax, which is then used to estimate elevation values for each pixel in the resulting DSM (Noh & Howat, 2017). In our study, a polygon-based landslide inventory was created for a subset area of the earthquake-affected region using high-resolution Worldview-3 imagery and SETSM-derived orthoimagery. Landslide identification involved visual analysis techniques on ortho-rectified optical imagery, focusing on features such as vegetation changes/removal, variations in reflectivity, and alterations in surface texture (Scaioni et al., 2014). First, we compared the pre- and post-event SETSM data with pre- and post-event LiDAR datasets in the coastal region where both datasets overlapped. Secondly, we compared the post-event SETSM topography with the post-event LiDAR data in the mountainous areas. We further classified sample regions into vegetated and non-vegetated to assess the influence of vegetation on the model comparisons. This analysis revealed a smaller average 3D distance for non-vegetated areas, indicating

a more precise alignment of data points for the LiDAR. The surface change detection model, created by differencing the pre- and post-event topography, was used to estimate the volume of displaced material for individual landslides. To ensure the accuracy of the volume estimates, we implemented several quality control measures. We established a threshold based on the maximum root mean square error (RMSE) from the point cloud alignment to identify areas with significant surface changes exceeding the 95% confidence level. Next, we differentiated the pre- and post-event point clouds within the validated surface change areas. This process involved separating points with negative elevation changes (representing loss of material) from points with positive changes (representing deposition). Subsequently, we performed a vertical difference analysis on each point cloud to determine the volume change associated with loss and deposition. Finally, we implemented a 0.3 volume-to-area (V/A) ratio threshold to distinguish between actual landslides and potential misinterpretations arising from factors like vegetation changes. The resulted V/A relationship between the mapped landslide area and the estimated volume from direct point cloud differencing was $VL = 1.82 \times AL^{1.16}$. The average loss area we identified was 1,178 m^2 and the maximum 130,494 m^2 (minimum 100 m^2). The analysis of the relationship between volume and area revealed a strong positive correlation between the two landslide variables (Pearson's $r = 0.89$, $p < 0.05$) in the AOI (Figure 1).

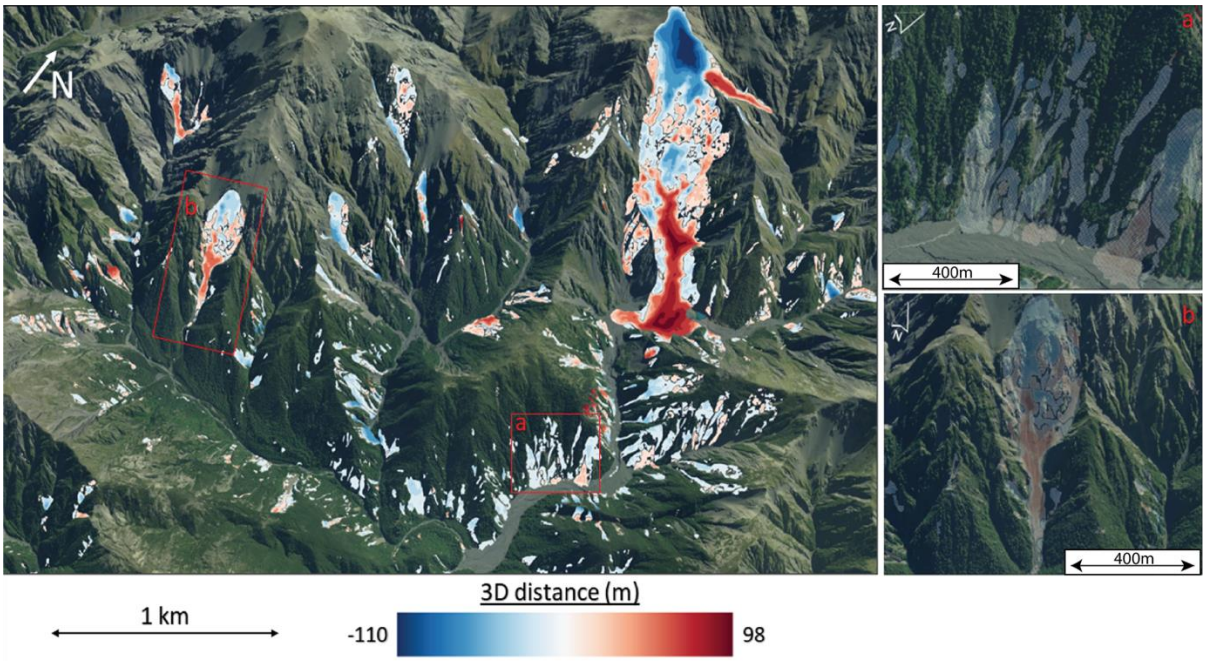

Figure 1. Map of the 3D signed distances from the geomorphic change detection phase between the pre-SETSM and the post-SETSM point clouds.

Conclusion

This study highlights the importance of topography in landslide modeling and proposes a comprehensive satellite-based approach for volume estimation, considering both frequent small landslides and impactful larger events. We identified 1,448 landslides, mostly narrow debris flows, with deep-seated landslides creating dam lakes. Topography registration accuracy varied between vegetated and non-vegetated areas, with the latter showing better alignment. 3D calculations revealed meter-scale erosion and deposition post-earthquake. We established a volume-to-area threshold to avoid overestimation and achieved meter scale volume calculations using pre- and post-event data. This research emphasizes the need for a holistic approach to landslide management, and innovations like SETSM and 3D distance mapping contribute to detailed analysis for rapid response and long-term planning. The findings stress the importance of continuous methodological development for accurate 3D landslide analysis, paving the way for improved preparedness and safety in landslide-prone areas.

References

Corominas, Jordi, and José Moya. "A review of assessing landslide frequency for hazard zoning purposes." *Engineering geology* 102.3-4 (2008): 193-213

Hamling, Ian J., et al. "Complex multifault rupture during the 2016 M w 7.8 Kaikōura earthquake, New Zealand." *Science* 356.6334

Massey, C., et al. "Landslides triggered by the 14 November 2016 Mw 7.8 Kaikōura earthquake, New Zealand." *Bulletin of the Seismological Society of America* 108.3B (2018): 1630-1648

Massey, C. I., et al. "Volume characteristics of landslides triggered by the MW 7.8 2016 Kaikōura Earthquake, New Zealand, derived from digital surface difference modeling." *Journal of Geophysical Research: Earth Surface* 125.7 (2020)

Petley, David. "Global patterns of loss of life from landslides." *Geology* 40.10 (2012): 927-930

Larsen, Isaac J., David R. Montgomery, and Oliver Korup. "Landslide erosion controlled by hillslope material." *Nature Geoscience* 3.4 (2010): 247-251

REFINING HYDRAULIC CONDUCITIVITY ESTIMATION IN FRACTURED MEDIA USING X-RAY TOMOGRAPHY, DISCRETE FRACTURE NETWORKS AND FLEXIBLE WALL PERMEAMETER

ELISA MAMMOLITI [1], DAVIDE FRONZI [1], MIRKO FRANCIONI [2], STEFANO MAZZOLI [3], JONATHAN DOMIZI[1], MATTEO RAPAZZETTI[1], ALESSIA CAPUTO[4], ALBERTO TAZIOLI[1], GIUSEPPE SCARPELLI[1], PAOLO CASTELLINI[4]

[1] *Department of Science, Matter Engineering, Environment and Urban Planning, Marche Polytechnics University, Italy, e.mammoliti@staff.univpm.it*

[2] *Department of Pure and Applied Sciences, University of Urbino, Italy*

[3] *School of Science and Technology, University of Camerino, Italy*

[4] *Department of Industrial Engineering and Mathematical Sciences, Marche Polytechnics University, Italy*

Introduction

Measuring hydraulic conductivity in fractured media is fundamental for several engineering applications including slope stability calculations and modelling of groundwater flow; however, it is also challenging due to varying discontinuities in aperture, roughness, and connectivity (Berkowitz, 2002; Mammoliti et al., 2023). Although traditional permeameter tests are able to capture data, they struggle with fracture complexity (Witherspoon et al., 1980). Recent advances in 3D X-ray tomography provide non-destructive, high-resolution imaging for detailed fracture analysis, precisely measuring discontinuity apertures and roughness to enhance fluid flow understanding (Glad et al., 2023). This study integrates 3D X-ray tomography with fracture analysis and DFN models to improve predictive accuracy of hydraulic conductivity in the Scaglia Rossa formation, a major fractured carbonate formation in the Umbria-Marche succession.

Methods

Standard flexible wall permeameter tests were used to measure the hydraulic conductivity of rock samples by imposing water flow and monitoring inflow, outflow, and differential pressure. High-resolution 3D X-ray tomography provided a 3D dataset of the fracture network, including fracture roughness and aperture. Discontinuities were classified from a geo-structural perspective, and aperture and roughness were manually measured using JRC (Barton, 1977) and an optical comparator to validate tomography data. Three DFN models were developed, using: (1) all identified discontinuities and manually extracted P21 values, (2) exclusively open discontinuities and manually extracted P21 values, and (3) open discontinuities and P32 values from 3D X-ray tomography (still under development).

Results

Fracture analysis revealed varying hydraulic conductivity essentially controlled by rock discontinuities (joints, veins, stylolites), with negligible flow within the matrix. Joints filled with clay, as well as pressure solution cleavage (tectonic stylolites) showed minimal enhancement in water flow due to reduced aperture and impervious filling. Conversely, open joints with favourable orientation for water flow exhibited higher hydraulic conductivity values, serving as preferential flow paths. Photogrammetric methods were used for fractures analysis using high-res photos processed into 3D models, to determine fracture intensity parameters (Figure 1a). Many fractures were closely spaced and filled with low-permeability materials, limiting groundwater flow. Clear-open joints exhibited pronounced water flow aligning coherently with their geometry. Detailed fracture characterization, integrating 3D X-ray tomography (Figure 1b), provided crucial insights into discontinuities pattern, aperture and roughness (Figure 1c), supporting permeameter results and allowing us to obtain improved physically based DFN models for water flow in fractured rock formations.

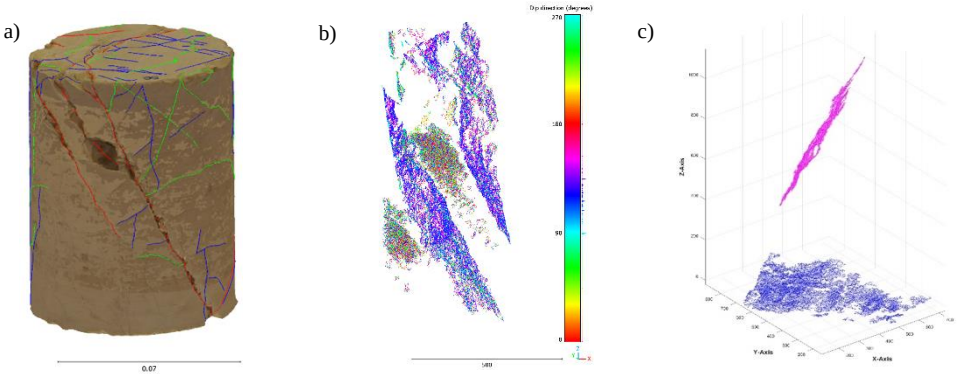

Figure 1. Example of discontinuity extraction and analysis. **(**a) Fracture network characterizing rock sample (used for fracture intensity calculation). (b) Extraction of rock discontinuities from 3D X-ray tomography. (c) Data post-processing for roughness calculation.

Conclusion

This study highlights the importance of combining standard testing with advanced imaging and modelling to accurately predict hydraulic conductivity in fractured rocks. Measuring roughness and aperture via 3D X-ray tomography enhances DFN models and hydraulic conductivity predictions. Flexible wall permeameter tests validate DFN-derived conductivity. Although currently ongoing, this research suggests that integrating 3D X-ray tomography could be crucial for groundwater management and engineering applications in fractured rock environments. Future work will focus on classifying rock bridges using tomographic methods.

References

Barton, N., & Choubey, V. The shear strength of rock joints in theory and practice. Rock mechanics. 1977, 10, 1-54.

Berkowitz, B. Characterizing flow and transport in fractured geological media: A review. Adv. Water Resour. 2002, 25 (8–12), 861–884.

Glad, A. C.; Afrough, A.; Amour, F.; Ferreira, C. A.; Price, N.; Clausen, O. R.; Nick, H. M. Anatomy of fractures: Quantifying fracture geometry utilizing X-ray computed tomography in a chalk-marl reservoir; the Lower Cretaceous Valdemar Field (Danish Central Graben). Journal of Structural Geology. 2023, 174, 104936

Mammoliti, E.; Pepi, A.; Fronzi, D.; Morelli, S.; Volatili, T.; Tazioli, A.; Francioni M. 3D Discrete Fracture Network Modelling from UAV Imagery Coupled with Tracer Tests to Assess Fracture Conductivity in an Unstable Rock Slope: Implications for Rockfall Phenomena. Remote Sensing. 2023, 15(5), 1222.

Witherspoon, P. A.; Wang, J. S.; Iwai, K.; & Gale, J. E. Validity of cubic law for fluid flow in a deformable rock fracture. Water resources research. 1980, 16(6), 1016-1024.